

- 1 • Article type: paper.
- 2 • Date text written or revised: 16 Nov 2017
- 3 • Number of words: 4548
- 4 • Number of figures: 15
- 5 • Number of tables: 2

6 -----

7 **Vision-based systems for structural deformation measurement: case studies**

8 Author 1

- 9 • Yan Xu* BEng, MEng
- 10 • Research Student, Vibration Engineering Section, College of Engineering, Mathematics and
- 11 Physical Sciences, University of Exeter, UK, EX4 4QF
- 12 • ORCID: 0000-0001-5886-9938

13 Author 2

- 14 • James Mark William Brownjohn BSc, PhD, DEng, CEng, FIMechE, FStructE
- 15 • Professor of Structural Dynamics, Vibration Engineering Section, College of Engineering,
- 16 Mathematics and Physical Sciences, University of Exeter, UK, EX4 4QF
- 17 • ORCID: 0000-0003-4946-5901

18 Full contact details of corresponding author (*)

19 Vibration Engineering Section, College of Engineering, Mathematics and Physical Sciences,
20 University of Exeter, UK, EX4 4QF

21 +44(0)1392726421

22 yx298@exeter.ac.uk

23

24 **ABSTRACT**

25 Vision-based systems offer a promising way for displacement measurement and receive increased
26 attention in civil structural monitoring. However, the working performance of vision-based systems,
27 especially the measurement accuracy and the robustness to different field conditions is not fully

28 understood. This study reports three cases studies of vision-based monitoring tests including one in a
29 laboratory, one on a short-span bridge and one on a long-span bridge. The tracking accuracy is
30 quantified in laboratory conditions in the range of 0.02 pixel to 0.20 pixel depending on the target
31 patterns as well as the tracking method selected. The measurement performance under several field
32 challenges are investigated including long-range measurement (e.g. camera-to-target distance at 710 m),
33 low-contrast target patterns, changes of target patterns and changes in lighting conditions. Three
34 representative tracking methods for the video processing, i.e. correlation-based template matching,
35 Lucas Kanade (LK) optical flow estimation and scale-invariant feature transform (SIFT) were used for
36 analysis, indicating their advantages and shortcomings for field measurement. One of the main
37 observations in field application is that changes in lighting conditions might cause some low-frequency
38 measurement error that could be misunderstood without the prior knowledge about structural loading
39 conditions.

40

41 Keywords

42 Bridges; Field testing & monitoring; Noise.

43

44 1 INTRODUCTION

45 Bridges provide vital links in transportation networks and must be managed in a manner that minimises
46 risk to public safety and disruption to service. However, the current inspection process mainly relies on
47 visual check that can be subjective and prone to error. Therefore, reliable approaches for bridge
48 condition assessment are required to assist the decision-making and make the best use of limited
49 maintenance budget.

50 Bridge deformation is a significant metric for bridge condition assessment. For example, measurement
51 of deformation during controlled vehicle load testing helps to estimate bridge load carrying capacity
52 (Wang et al., 2011) (BBC News, 2015). Serviceability is reflected through deformation during normal
53 operation, since extreme values and ranges indicate problems that may limit operational use.

54 *1.1 Review of vision-based approaches*

55 Limitations of more traditional displacement sensing technologies (e.g. LVDT, GPS, double-integration
56 from acceleration etc.) that necessarily require physical access to a structure have driven research in
57 non-contact optical sensing. Vision-based monitoring methods have promising features e.g. simple
58 instrumentation and installation, operation remote from the structure and capacity for multi-point
59 measurement using a single (camera) sensor. Existing studies have indicated the potential of vision-
60 based methods for structural condition assessment, in particular for system identification (Caetano et
61 al., 2007; Oh et al., 2015; Yoon et al., 2016), finite element model calibration (Feng and Feng, 2015),
62 damage detection (Cha et al., 2017) and contribution to bridge WIM system with camera assistance for
63 traffic monitoring (Ojio et al., 2016).

64 Target tracking is one critical component in a vision-based system, directly influencing the
65 measurement accuracy. Template matching (Brownjohn et al., 2017; Chang and Ji, 2007; Ehrhart and
66 Lienhart, 2015a; Fukuda et al., 2013; Guo and Zhu, 2016; Macdonald et al., 1997; Stephen et al., 1993)
67 and optical flow estimation (Caetano et al., 2011; Cha et al., 2017; Chen, Wu, et al., 2015; Chen et al.,
68 2017; Chen, Wadhwa, et al., 2015; Diamond et al., 2017; Ehrhart and Lienhart, 2015b; Ji and Chang,
69 2008a; Khaloo and Lattanzi, 2017; Yang et al., 2017; Yoon et al., 2016) are established methods widely
70 used for bridge deformation measurement whereas feature point matching is a relatively new and
71 promising tracking method that is theoretically scale-invariant and rotation-invariant (Ehrhart and
72 Lienhart, 2015a) and has been validated in several short-range measurement tests (Ehrhart and Lienhart,
73 2015a, 2015b, Khuc and Catbas, 2017a, 2017b). There are also some other methods through tracking
74 the special shapes of target patterns based on edge detection or image thresholding algorithms (Ji and
75 Chang, 2008b; Lee et al., 2006; Ribeiro et al., 2014; Wahbeh et al., 2003) e.g. line-like cables, circular-
76 shaped dots and chessboard, etc. These methods have limitations for application due to the requirement
77 about pattern shapes.

78 To find the most appropriate tracking method for structural monitoring, it is necessary to evaluate their
79 measurement accuracy and the robustness to different field conditions. Busca et al. (Busca et al., 2014)
80 evaluated three techniques (template matching, edge detection and digital image correlation) on a steel

81 truss railway bridge, concluding that the three techniques provide similar tracking performance while
82 tracking accuracy is slightly poorer for natural targets. Ehrhart and Lienhart (Ehrhart and Lienhart,
83 2015a) evaluated the performance of three techniques (optical flow, template matching and feature point
84 matching) by tracking structural features of a footbridge and reported that feature point matching is
85 robust to the changes of background condition (i.e. snowfall) whereas drift over time was observed in
86 the measurement by two other methods.

87 These two existing studies provide some information about the influence of pattern features and pattern
88 changes on measurement results. However, more studies are necessary to evaluate the field performance
89 of vision-based systems since several critical field challenges are not considered yet e.g. robustness to
90 lighting changes and viability for long-range monitoring.

91 *1.2 Purpose of this study*

92 The purpose of this study is to investigate the effectiveness of vision-based systems for displacement
93 measurement in different environmental conditions through three case studies. One laboratory test and
94 two field tests were performed indicating several influential factors on measurement performance, i.e.
95 estimation error in projection transformation, camera-to-target distance, the distinctiveness of target
96 patterns, changes of target patterns and changes in lighting conditions. Three representative tracking
97 methods were considered for video processing, demonstrating their advantages and shortcomings to
98 deal with the observed influential factors. Other error sources in field tests like camera shake,
99 atmospheric refraction and temperature variations were not apparent in test observations and thus are
100 not discussed in this study.

101 This paper is the first study to apply the feature point matching method in the long-range monitoring
102 test and the measurement was evaluated through comparison with the processing results using classical
103 tracking methods. The field measurement by vision-based systems might carry some low-frequency
104 error due to camera shake or lighting changes. A method to distinguish the main source of low frequency
105 error is proposed in this study.

106 To that end, section 2 introduces the methodologies for vision-based displacement measurement, in
107 particular, three representative tracking methods. In section 3, a laboratory uniaxial oscillation test used

108 to validate the video processing methods and to study the tracking accuracy in laboratory conditions is
109 described. Section 4 and 5 report the field tests for mid-span deformation measurement in a short-span
110 railway bridge and a long-span suspension bridge, respectively. The performance of vision-based
111 systems with challenging field conditions e.g. low-contrast patterns, changes of target patterns and
112 changes in lighting conditions are investigated, indicating the advantages and shortcomings of the three
113 tracking methods. Finally the main findings from the three tests are summarised.

114

115 2 VIDEO PROCESSING METHODOLOGIES

116 In vision-based systems, the hardware comprises data acquisition devices, portable computer with video
117 processing software and accessories like tripod and artificial targets (optional). Video processing
118 package is the key part which could fit into a three-component framework in Figure 1, i.e. camera
119 calibration, target tracking and displacement calculation.

120 Camera calibration is aimed at determining the projection transformation from the structural system to
121 the image plane. The projection transformation used in this study is the planar homography that is
122 calibrated based on a few planar point correspondences and is capable to reconstruct the two-
123 dimensional planar displacement.

124 Target tracking is critical in the video processing package to locate the target regions in the image plane
125 through tracking methods. The tracking methods considered in this study include template matching
126 and optical flow estimation that are established and classic, as well as feature point matching that
127 receives increased attention in structural monitoring.

128 The structural displacement could be easily derived from the change of structural coordinates given the
129 image location of a target (output of target tracking) and a projection transformation (output of camera
130 calibration).

131 A software package for the post-processing analysis of video files to measure the structural
132 displacement is developed by the authors using C++ language, partly referring to OpenCV library. This
133 custom-developed software is capable to measure the structural displacement of multiple targets

134 simultaneously within the field of view and offers three options of tracking methods (shown in Figure
135 1) to adapt to different test conditions.

136 This section provides a description of the methodologies of three target tracking methods used in the
137 custom-developed video-processing software i.e. correlation-based template matching, Lucas Kanade
138 (LK) optical flow estimation and scale-invariant feature transform (SIFT) method (Lowe, 2004).

139 2.1 *Correlation-based template matching*

140 Template matching is a classic technique for target tracking by searching in a new frame for an area
141 most closely resembling a predefined template, following the procedures demonstrated in Figure 2. A
142 target region is selected as the template that is a subset image in the reference frame. A matching
143 criterion is defined to evaluate the similarity degree between the template and the new frame and the
144 criterion used is zero-mean normalised cross correlation coefficient (ZNCC). The target location in the
145 new frame corresponds to the peak location in the similarity matrix that has resolution at pixel level.
146 Subpixel interpolation schemes (Feng et al., 2015) are required to refine the tracking results to sub-pixel
147 level and the interpolation method used in this study is zero-padding in frequency domain using the
148 matrix multiplication form of discrete Fourier transform (Guizar-Sicairos et al., 2008).

149 Template matching has been applied in structural monitoring since the earliest work on the Humber and
150 Severn Bridges in 1990s (Macdonald et al., 1997; Stephen et al., 1993), and the recent applications
151 include displacement monitoring tests in a railway bridge (Feng et al., 2015), a long-span bridge (Ye et
152 al., 2013) and a high-rise building (Liao et al., 2010).

153 2.2 *Lucas Kanade optical flow estimation*

154 Lucas Kanade optical flow estimation detects the motions in an image from the brightness pattern shift
155 (Beauchemin and Barron, 1995). The calculation process imposes one temporal constraint on image
156 properties and one spatial constraint on motion consistency, i.e. that the pixel intensities of an object do
157 not change between consecutive frames and that neighbouring pixels have similar motion. The image
158 motions are derived using the following equation,

$$159 \begin{bmatrix} dx \\ dy \end{bmatrix} = \begin{bmatrix} \sum_i I_{xi}^2 & \sum_i I_{xi} I_{yi} \\ \sum_i I_{xi} I_{yi} & \sum_i I_{yi}^2 \end{bmatrix}^{-1} \begin{bmatrix} -\sum_i I_{xi} I_{ti} \\ -\sum_i I_{yi} I_{ti} \end{bmatrix} \quad (1)$$

160 where dx and dy denote the motions in image plane; I_x , I_y and I_t represent the spatial and temporal
161 gradients of image intensities; and i denotes the i th pixel location in a 3×3 patch around a feature point
162 (x, y) .

163 The procedures are demonstrated in Figure 3. The most prominent corners are detected by Shi-Tomasi
164 corner detector (Jianbo Shi and Tomasi, 1994) in the reference frame with their locations updated in the
165 new frame by Eq.(1). Backward estimation is then performed from the new frame to the reference frame
166 in order to refine the point correspondences based on the error between the initially detected points and
167 the backward-estimated points. Point correspondences are further refined based on geometric alignment
168 using the least median of squares method (Massart et al., 1986).

169 The LK optical flow estimation was applied in a laboratory test of a multi-storey metal tower (Yoon et
170 al., 2016) for system identification, for field application of a footbridge deformation monitoring
171 (Ehrhart and Lienhart, 2015b) and for bridge stay-cable vibration measurement (Caetano et al., 2011;
172 Ji and Chang, 2008a).

173 2.3 Scale-invariant feature transform (SIFT)

174 Feature point matching is an efficient tracking technique through matching feature points in consecutive
175 images based on their local appearance. Several robust feature extractors and descriptors are reported
176 in literature (Alahi et al., 2012; Bay et al., 2008; Calonder et al., 2010; Lowe, 2004; Rublee et al., 2011)
177 and the one used in this study is the SIFT method.

178 The procedures are demonstrated in Figure 4. Keypoints are extracted from the local extremes in the
179 Difference of Gaussian images (differences of Gaussian filtered images with varied blur level) and
180 described by vectors using the gradient magnitudes and orientations of neighbouring pixels. Keypoints
181 between two images are matched by identifying their nearest neighbours evaluated using the Euclidean
182 distances between keypoint descriptor vectors. The outliers in keypoint correspondences are removed
183 based on geometric alignment using the least median of squares method (Massart et al., 1986).

184 The SIFT method has been validated in the deformation measurement test of a railway bridge (Khuc
185 and Catbas, 2017a). Other feature point matching methods are also validated only in short-range
186 monitoring tests (Ehrhart and Lienhart, 2015a, 2015b; Khuc and Catbas, 2017b).

187 3 VALIDATION TEST IN CONTROLLED ENVIRONMENT

188 This section investigates the performance of three tracking methods (i.e. correlation-based template
189 matching, LK optical flow estimation and SIFT method) in controlled environmental conditions through
190 a laboratory uniaxial oscillation test.

191 *3.1 Test configuration*

192 An APS 400 Electrodynamic shaker was set vertically on solid ground shown in Figure 5(a) and driven
193 by an input of chirp signal with frequency range 0.5 Hz to 2 Hz. The test was run twice, with no artificial
194 target in Run 1 and with the chessboard pattern attached to shaker mass (shown in Figure 5(b)) in Run
195 2 in order to increase the feature salience.

196 One GoPro Hero4 camera was fixed on the ground looking at the oscillating shaker mass; sample frames
197 in two runs are given in (c) and (d). The frame rate was set as nominally 60 Hz with narrow field-of-
198 view option. A Balluff micropulse transducer was attached to the shaker mass shown in (b) to provide
199 an accurate reference displacement measurement sampled at 256 Hz.

200 The recorded video files were post-processed using the custom-developed video processing software to
201 derive the displacement data of shaker mass. Camera calibration was performed according to the
202 dimensions of shaker mass indicated in Figure 5(b) to estimate the planar homography; the target
203 locations in the image were estimated by the three tracking methods, respectively; and the horizontal
204 and vertical displacement was acquired through transforming the image locations to the structural
205 locations via the planar homography.

206 *3.2 Measurement results*

207 The measurement results using the GoPro camera and Balluff transducer in two runs are illustrated in
208 Figure 6, indicating that,

- 209 • Vision-based system based on a consumer-grade camera is qualified to measure the vertical
210 oscillation of shaker mass by tracking either natural features or artificial target patterns with the
211 cross-correlation coefficient (compared with the Balluff measurement) reaching over 99%.
- 212 • Oscillation occurred only in the vertical direction and any displacement measurement in the
213 horizontal direction corresponds to measurement error. In Run 1, correlation-based template

214 matching provides the best measurement performance while the SIFT measurement includes the
215 highest noise. Measurement error in Run 2 is much smaller than in Run 1 after increasing the target
216 salience.

- 217 • During the oscillation period in Run 2, the horizontal measurement indicates a chirp signal with a
218 similar shape as the vertical measurement but with much smaller amplitude. It might be caused by
219 the error in projection transformation, making the dominant vibration leak to minor motion
220 direction.

221 To investigate the tracking accuracy of the three methods, the data collected during the stationary period
222 were taken into account with the estimation results summarised in Table 1. This indicates that in
223 laboratory conditions, correlation-based template matching is the most accurate method while the SIFT
224 achieves the poorest accuracy with the highest sensitivity to the distinctiveness of target patterns.

225 Laboratory evaluation avoids numerous difficulties that can diminish performance in field conditions
226 due to environmental influences such as camera-to-target distance, unstable target patterns and lighting
227 conditions, etc. In section 4 and 5, two field tests on bridge deformation measurement are reported to
228 illustrate the real-world working performance of vision-based systems.

229 4 DEFORMATION MEASUREMENT TEST ON A SHORT-SPAN BRIDGE

230 The vision-based system applied in the two field tests is the Imetrum Dynamic Monitoring Station
231 (DMS) originating from research at the University of Bristol and commercialised via the university
232 spin-out company Imetrum formed in 2003. The system includes one or more GigE high performance
233 cameras for data acquisition and the software ‘Video Gauge’ for the real-time video processing.

234 The target tracking algorithms used in the software are proprietary extensions of correlation-based
235 template matching techniques which enable better than 1/100 pixel resolution at sample rates beyond
236 100 Hz in field applications. The system used by University of Exeter has been trialled in several one-
237 day field campaigns on a number of bridges in the UK, indicating comparable or even better
238 measurement accuracy compared to an LVDT for short-range measurement (Hester et al., 2017) and
239 the GPS for long-range measurement (Xu et al., 2017).

240 In this study, the Imetrum system was used in field tests mainly for two functions, 1) as a data
241 acquisition device to record the video files of the bridges that would be analysed using the custom-
242 developed video processing software, and 2) to provide (using the Imetrum proprietary video processing
243 software) the reference data of bridge deformation for the evaluation of the measurement results
244 provided by the custom-developed video processing software.

245 This section reports a case study using the vision-based system for the deformation measurement of a
246 short-span railway bridge. Section 4.1 and 4.2 below describe the test setup and the results obtained,
247 respectively.

248 *4.1 Test configuration*

249 The Mineral Line Bridge is a steel girder bridge with 14 m span, carrying the West Somerset Railway
250 near Watchet, UK. Figure 7(a) indicates the test setup with an Imetrum camera mounted at the top of a
251 tripod approximately 12.5 m away from the mid-span of the bridge. One sample frame captured by the
252 Imetrum camera is illustrated in Figure 7(b) with the target region for measurement marked by a
253 rectangular box.

254 Since the fundamental frequency of the bridge was estimated to be above 10 Hz, a frame rate of 30 Hz
255 was set for the Imetrum system. The camera calibration was performed using the dimensions of the
256 bridge girder and the artificial target at mid-span. The displacement data along the vertical and
257 longitudinal directions was measured directly by the Imetrum system and also extracted from the
258 custom-developed post-processing software using the three tracking methods.

259 *4.2 Measurement results*

260 Time history data of displacement measurement are illustrated in Figure 8, indicating that,

- 261 • The three tracking methods all capture the vertical deformation of the bridge induced by the passing
262 of a steam train with one steam locomotive and seven passenger carriages with the maximum
263 deformation at 6.4 mm.
- 264 • A similar deformation pattern during the train passing occurs in the longitudinal measurement with
265 much smaller amplitudes (less than 0.56 mm) apart from the measurement by SIFT method due to

266 the high noise. It might be caused by the error of projection transformation, making the vertical
267 deflection data leaked to the horizontal direction.

268 • An apparent low-frequency motion trend in the horizontal direction is observed after 30 s for all the
269 four measurement that should be an error since the bridge was empty with no heavy loading. During
270 this period, the four methods provide different amplitude values and the SIFT measurement is the
271 most noisy one but with the smallest amplitude. The LK optical flow estimation method failed to
272 measure in some frames possibly due to the large brightness changes. In terms of the image motion,
273 the maximum drift in the image horizontal direction reaches approx. 0.3 pixel, larger than the
274 estimated tracking accuracy in laboratory conditions. It indicates that the tracking accuracy
275 becomes poorer in field conditions for any of the three tracking methods.

276 According to the authors' test experiences and the literature, the low-frequency error in vision-based
277 measurement could be caused by either the camera motion (Zhao et al., 2017) or changes in lighting
278 conditions (Brownjohn et al., 2017). The error induced by camera motion should be consistent at those
279 pixels corresponding to the stationary objects in the field of view. The camera motion is believed not to
280 be the main error source in this case because Figure 8 is for one among several targets tracked in the
281 bridge girder (in Figure 9(a)), and these show image motions inconsistent in both the amplitude and
282 direction as shown in Figure 9(b) and (c).

283 To quantify the influence of lighting changes, mean pixel intensity at the initially selected target region
284 (T0) were calculated as shown in Figure 10(a). This indicates a growth of averaged brightness from
285 28.5 s to 37 s followed by a gentle decrease, which has a trend similar to the measurement error in the
286 longitudinal direction in Figure 8(a). The initial frame and the frame at the time step 37 s are shown in
287 Figure 10(b) and (c) for visual comparison of lighting changes. In the second frame, the bolts within
288 the rectangular region (T0) are more distinctive against the background due to the improved lighting.
289 Therefore, it is believed that the low-frequency error in the longitudinal direction is caused by the
290 lighting changes.

291 None of the three tracking methods is robust to large lighting changes in field tests. The SIFT method
292 experiences the least influence in measurement while the LK optical flow might fail to identify the

293 features under apparent lighting changes. The low-frequency error due to lighting changes might
294 mislead the users about the bridge loading condition if no prior knowledge is available.

295 A sharp brightness increase is observed at time step 18.57 s in Figure 10(a) corresponding to an outlier
296 in the measurement by correlation-based template matching and the Imetrum system in Figure 8. The
297 cause of these anomalies is changes in target pattern due to a bird flying in front of the target, as shown
298 in Figure 11. This indicates that the LK optical flow estimation and SIFT method are not sensitive to
299 small pattern changes whereas the correlation-based template matching method might fail to track.

300 The demonstration of vision-based monitoring in a short-span bridge indicates that the vision-based
301 system is capable to measure the bridge deflection under traffic loads using any of the three tracking
302 methods, although the measurement might become unstable when suffering from apparent changes in
303 lighting conditions or target patterns.

304 In the next section, a similar test was performed on a long-span bridge to investigate the viability of
305 vision-based system for the long-range monitoring.

306 5 DEFORMATION MEASUREMENT TEST ON A LONG-SPAN BRIDGE

307 This section describes a case study of using a vision-based system measuring deformation of the
308 Humber Bridge, UK, a suspension bridge with (at the time of writing) the world's eighth longest span.
309 Section 5.1 and 5.2 describe the test setup and the results obtained, respectively. The Imetrum system
310 was used in field for video acquisition and the video files were post-processed by the custom-developed
311 software to evaluate the performance of three tracking methods for the long-range measurement.

312 5.1 Test configuration

313 The Humber Bridge, with main span of 1410 m links the towns of Hessle and Barton across the Humber
314 estuary. A single day of field testing using the Imetrum system on 22nd July 2015 was used to measure
315 the displacement at mid-span of the bridge which has been reported in (Brownjohn et al., 2017; Xu et
316 al., 2017). The camera, equipped with a lens of 300 mm focal length, was located at the base of the
317 north tower shown in Figure 12(a), 710 m from the mid-span of the bridge. An artificial target with the
318 pattern of concentric rings in Figure 12(b) was attached to the parapet at the mid-span. One sample

319 frame by vision-based system is shown in Figure 12(c) with the annotations at the two target regions,
320 T1 covering the artificial target region and T2 under the deck soffit with low-contrast patterns.
321 The previous modal test (Brownjohn et al., 2010) indicates 14 modes in the vertical direction with the
322 modal frequencies lower than 1 Hz and the fundamental frequency was 0.117 Hz. Since the frequency
323 components of interest were lower than 1 Hz, the frame rate of the Imetrum system was set as 10 Hz.
324 The camera calibration was performed according to the square dimension (1 m) of the artificial target.
325 The displacement data along the vertical and transverse directions was measured directly by the
326 Imetrum system and also extracted from the custom-developed post-processing software using the three
327 tracking methods.

328 5.2 *Measurement results*

329 An 80-second signal of vertical displacement at the target region T1 recorded at approx. 19.22 PM (BST)
330 is illustrated in Figure 13. The maximum displacement reaches 160.5 mm at approximately 31 s by the
331 Imetrum measurement while some data points using the three post-processing methods are missing for
332 about 0.9 s when the displacement values reach their maxima. Two frames during this period are shown
333 in Figure 14 indicating a big change in target pattern. Due to the low sun elevation in the west, the target
334 panel on the east side was initially partially in the shadow of the bridge railing, shown in (a). When one
335 tall vehicle passed the mid-span of the bridge between the sun and the target, sunlight was completely
336 blocked, making the whole target pattern visible in the image. This indicates that the three tracking
337 methods are all not robust to large changes in target patterns. Imetrum system, with its proprietary
338 algorithms, is more robust in this case.

339 The target region T2 is located at the deck soffit that is less salient with smaller spatial changes in target
340 patterns compared with the target region T1. In Figure 15, the maximum displacement measured at T2
341 is 128.2 mm and 130.7 mm by the correlation-based template matching and SIFT method, respectively
342 while the LK optical flow method failed to track several frames including the period reaching the
343 maximum displacement. This indicates that the LK optical flow method has higher requirements on
344 salience and stability of target patterns. The displacement measured at T2 is smaller than that measured
345 at T1 because 1) the two targets would experience different motion as the bridge rotates about its
346 longitudinal axis due to eccentric traffic loading; and 2) the bridge axis directions projected in the image

347 plane and the projection transformation were determined according to the artificial target panel and thus
348 were not perfectly aligned with those for the feature target T2 under the deck soffit.

349 6 CONCLUSIONS

350 This paper investigates the performance of vision-based systems for displacement measurement in
351 laboratory and field tests. Three representative tracking methods (i.e. correlation-based template
352 matching, LK optical flow estimation and SIFT method) were used for the post processing of test
353 records with their performance compared with a commercial vision-based system, Imetrum DMS.

354 In laboratory conditions, the tracking accuracies for the two methods, correlation-based template
355 matching and LK optical flow estimation are close varied from 0.02 pixel to 0.10 pixel depending on
356 target patterns while the accuracy of SIFT method is poorer in the range between 0.03 pixel and 0.20
357 pixel.

358 The working performance of three tracking methods in field tests are summarised in Table 2.

- 359 • All the three tracking methods are effective for either short range or long range measurement (e.g.
360 camera-to-target distance at 710 m) with the displacement varying from several millimetres to ten
361 centimetres. However, the tracking accuracy becomes poorer than that achieved in laboratory
362 conditions.
- 363 • The salience of target patterns has a direct influence on the measurement accuracy and high-contrast
364 patterns are preferred for tracking. LK optical flow estimation has the highest requirement about
365 the distinctiveness and stability of target patterns and might fail to track when the other two methods
366 work fine.
- 367 • Changes to target patterns due to object obstruction or daytime shadows might lead to missing data.
368 Correlation-based template matching is the method most sensitive to the changes of target patterns
369 while the other two tracking methods are also influenced when facing large changes on target
370 patterns.
- 371 • Changes of lighting conditions might cause some low-frequency measurement error using any of
372 the three tracking methods, which could be misunderstood without the prior knowledge of structural

373 loading. SIFT method is influenced by the lighting changes but provides smaller measurement error
374 compared with the other two methods.

375 It is indicated that apart from constraining the test conditions, e.g. testing in overcast weather or
376 selecting the sheltered target patterns, how to deal with varying lighting conditions in the field is still
377 an open question for vision-based measurement.

378 Another important observation is that although the two-dimensional displacement measurement is
379 provided by the vision-based system, the measurement along the minor deformed direction might not
380 be reliable. This is because the error in projection transformation might lead to the leakage of dominant
381 deformation to the minor deformed direction. Thus special attention should be given to interpret the
382 measured displacement along the minor deformed direction.

383 ACKNOWLEDGEMENT

384 We would like to thank the West Somerset Railway and the Humber Bridge Board for permission to
385 use their bridges and for assistance they provided. Also thanks to Farhad Huseynov and Karen Faulkner
386 for organising the field test in the Mineral Line Bridge. **Finally the authors would like to thank the two**
387 **anonymous reviewers for their constructive comments.**

388 REFERENCES

389 Alahi, A., Ortiz, R. and Vanderghenst, P. (2012), “Freak: Fast retina keypoint”, *IEEE Conference on*
390 *Computer Vision and Pattern Recognition (CVPR)*, pp. 510–517.

391 Bay, H., Ess, A., Tuytelaars, T. and Van Gool, L. (2008), “Speeded-up robust features (SURF)”,
392 *Computer Vision and Image Understanding*, Vol. 110 No. 3, pp. 346–359.

393 BBC News. (2015), “Lorry tests as monitors installed in Forth Road Bridge first”, *BBC News Web Site*,
394 available at: <http://www.bbc.co.uk/news/uk-scotland-edinburgh-east-fife-35151289> (accessed 21
395 December 2015).

396 Beauchemin, S.S. and Barron, J.L. (1995), “The computation of optical flow”, *ACM Computing Surveys*,
397 Vol. 27 No. 3, pp. 433–466.

398 Brownjohn, J.M.W., Magalhaes, F., Caetano, E. and Cunha, A. (2010), “Ambient vibration re-testing

399 and operational modal analysis of the Humber Bridge”, *Engineering Structures*, Vol. 32 No. 8, pp.
400 2003–2018.

401 Brownjohn, J.M.W., Xu, Y. and Hester, D. (2017), “Vision-Based Bridge Deformation Monitoring”,
402 *Frontiers in Built Environment*, Vol. 3, pp. 1–16.

403 Busca, G., Cigada, A., Mazzoleni, P. and Zappa, E. (2014), “Vibration Monitoring of Multiple Bridge
404 Points by Means of a Unique Vision-Based Measuring System”, *Experimental Mechanics*, Vol.
405 54, pp. 255–271.

406 Caetano, E., Silva, S. and Bateira, J. (2007), “Application of a vision system to the monitoring of cable
407 structures”, *Seventh International Symposium on Cable Dynamics*, pp. 225–236.

408 Caetano, E., Silva, S. and Bateira, J. (2011), “A vision system for vibration monitoring of civil
409 engineering structures”, *Experimental Techniques*, Vol. 35 No. 4, pp. 74–82.

410 Calonder, M., Lepetit, V., Strecha, C. and Fua, P. (2010), “Brief: Binary robust independent elementary
411 features”, *European Conference on Computer Vision*, Crete, Greece, pp. 778–792.

412 Cha, Y.-J., Chen, J.G. and Büyüköztürk, O. (2017), “Output-only computer vision based damage
413 detection using phase-based optical flow and unscented Kalman filters”, *Engineering Structures*,
414 Vol. 132, pp. 300–313.

415 Chang, C.C. and Ji, Y.F. (2007), “Flexible Videogrammetric Technique for Three-Dimensional
416 Structural Vibration Measurement”, *Journal of Engineering Mechanics*, Vol. 133 No. 6, pp. 656–
417 664.

418 Chen, C.-C., Wu, W.-H., Tseng, H.-Z., Chen, C.-H. and Lai, G. (2015), “Application of digital
419 photogrammetry techniques in identifying the mode shape ratios of stay cables with multiple
420 camcorders”, *Measurement*, Vol. 75, pp. 134–146.

421 Chen, J.G., Davis, A., Wadhwa, N., Durand, F., Freeman, W.T. and Buyukozturk, O. (2017), “Video
422 Camera-Based Vibration Measurement for Civil Infrastructure Applications”, *Journal of*
423 *Infrastructure Systems*, Vol. 23 No. 3, p. 11.

424 Chen, J.G., Wadhwa, N., Cha, Y.-J., Durand, F., Freeman, W.T. and Buyukozturk, O. (2015), “Modal
425 identification of simple structures with high-speed video using motion magnification”, *Journal of*
426 *Sound and Vibration*, Vol. 345, pp. 58–71.

427 Diamond, D.H., Heyns, P.S. and Oberholster, A.J. (2017), “Accuracy evaluation of sub-pixel structural
428 vibration measurements through optical flow analysis of a video sequence”, *Measurement*, Vol.
429 95, pp. 166–172.

430 Ehrhart, M. and Lienhart, W. (2015a), “Monitoring of Civil Engineering Structures using a State-of-
431 the-art Image Assisted Total Station”, *Journal of Applied Geodesy*, Vol. 9 No. 3, pp. 174–182.

432 Ehrhart, M. and Lienhart, W. (2015b), “Development and evaluation of a long range image-based
433 monitoring system for civil engineering structures”, in Shull, P.J. (Ed.), *Proc. SPIE Structural
434 Health Monitoring and Inspection of Advanced Materials, Aerospace, and Civil Infrastructure*,
435 Vol. 9437, San Diego, California, United States, p. 94370K.

436 Feng, D., Feng, M., Ozer, E. and Fukuda, Y. (2015), “A Vision-Based Sensor for Noncontact Structural
437 Displacement Measurement”, *Sensors*, Vol. 15 No. 7, pp. 16557–16575.

438 Feng, D. and Feng, M.Q. (2015), “Model Updating of Railway Bridge Using In Situ Dynamic
439 Displacement Measurement under Trainloads”, *Journal of Bridge Engineering*, Vol. 20 No. 12,
440 pp. 1–12.

441 Fukuda, Y., Feng, M.Q., Narita, Y., Kaneko, S. and Tanaka, T. (2013), “Vision-Based Displacement
442 Sensor for Monitoring Dynamic Response Using Robust Object Search Algorithm”, *IEEE Sensors
443 Journal*, Vol. 13 No. 12, pp. 4725–4732.

444 Guizar-Sicairos, M., Thurman, S.T. and Fienup, J.R. (2008), “Efficient subpixel image registration
445 algorithms”, *Optics Letters*, Vol. 33 No. 2, pp. 156–158.

446 Guo, J. and Zhu, C. (2016), “Dynamic displacement measurement of large-scale structures based on the
447 Lucas–Kanade template tracking algorithm”, *Mechanical Systems and Signal Processing*, Vol.
448 66–67, pp. 425–436.

449 Hester, D., Brownjohn, J., Bocian, M. and Xu, Y. (2017), “Low cost bridge load test: calculating bridge
450 displacement from acceleration for load assessment calculations”, *Eng. Struct.*, Vol. 143, pp. 358–
451 374.

452 Ji, Y.F. and Chang, C.C. (2008a), “Nontarget Image-Based Technique for Small Cable Vibration
453 Measurement”, *Journal of Bridge Engineering*, Vol. 13 No. 1, pp. 34–42.

454 Ji, Y.F. and Chang, C.C. (2008b), “Nontarget Stereo Vision Technique for Spatiotemporal Response

455 Measurement of Line-Like Structures”, *Journal of Engineering Mechanics*, Vol. 134 No. 6, pp.
456 466–474.

457 Jianbo Shi and Tomasi. (1994), “Good features to track”, *Proceedings of IEEE Conference on*
458 *Computer Vision and Pattern Recognition CVPR-94*, IEEE Comput. Soc. Press, pp. 593–600.

459 Khaloo, A. and Lattanzi, D. (2017), “Pixel-wise structural motion tracking from rectified repurposed
460 videos”, *Structural Control and Health Monitoring*, Vol. 24 No. 11, p. e2009.

461 Khuc, T. and Catbas, F.N. (2017a), “Computer vision-based displacement and vibration monitoring
462 without using physical target on structures”, *Structure and Infrastructure Engineering*, Vol. 13
463 No. 4, pp. 505–516.

464 Khuc, T. and Catbas, F.N. (2017b), “Completely contactless structural health monitoring of real-life
465 structures using cameras and computer vision”, *Structural Control and Health Monitoring*, Vol.
466 24 No. 1, p. e1852.

467 Lee, J.J., Cho, S., Shinozuka, M., Yun, C., Lee, C.-G. and Lee, W.-T. (2006), “Evaluation of Bridge
468 Load Carrying Capacity Based on Dynamic Displacement Measurement Using Real-time Image
469 Processing Techniques”, *Steel Structures*, Vol. 6 No. 5, pp. 377–385.

470 Liao, W.Y., Chen, W.H., Ni, Y.Q. and Xia, Y. (2010), “Development of a vision-based real-time
471 displacement measurement system for Guangzhou New TV Tower”, in Casciati, F. and Giordano
472 M. (Eds.), *Proceedings of the 5th European Workshop on Structural Health Monitoring*, Sorrento,
473 Naples, Italy, pp. 450–455.

474 Lowe, D.G. (2004), “Distinctive image features from scale-invariant keypoints”, *International Journal*
475 *of Computer Vision*, Springer, Vol. 60 No. 2, pp. 91–110.

476 Macdonald, J.H.G., Dagless, E.L., Thomas, B.T. and Taylor, C.A. (1997), “Dynamic measurements of
477 the Second Severn Crossing”, *Proceedings of the Institution of Civil Engineers - Transport*, Vol.
478 123 No. 4, pp. 241–248.

479 Massart, D.L., Kaufman, L., Rousseeuw, P.J. and Leroy, A. (1986), “Least median of squares: a robust
480 method for outlier and model error detection in regression and calibration”, *Analytica Chimica*
481 *Acta*, Vol. 187 No. C, pp. 171–179.

482 Oh, B.K., Hwang, J.W., Kim, Y., Cho, T. and Park, H.S. (2015), “Vision-based system identification

483 technique for building structures using a motion capture system”, *Journal of Sound and Vibration*,
484 Elsevier, Vol. 356, pp. 72–85.

485 Ojio, T., Carey, C.H., OBrien, E.J., Doherty, C. and Taylor, S.E. (2016), “Contactless Bridge Weigh-
486 in-Motion”, *Journal of Bridge Engineering*, American Society of Civil Engineers, Vol. 21 No. 7,
487 p. 4016032.

488 Ribeiro, D., Calçada, R., Ferreira, J. and Martins, T. (2014), “Non-contact measurement of the dynamic
489 displacement of railway bridges using an advanced video-based system”, *Engineering Structures*,
490 Vol. 75, pp. 164–180.

491 Rublee, E., Rabaud, V., Konolige, K. and Bradski, G. (2011), “ORB: An efficient alternative to SIFT
492 or SURF”, *Proceedings of the IEEE International Conference on Computer Vision*, IEEE, pp.
493 2564–2571.

494 Stephen, G.A., Brownjohn, J.M.W. and Taylor, C.A. (1993), “Measurements of static and dynamic
495 displacement from visual monitoring of the Humber Bridge”, *Engineering Structures*, Elsevier,
496 Vol. 15 No. 3, pp. 197–208.

497 Wahbeh, A.M., Caffrey, J.P. and Masri, S.F. (2003), “A vision-based approach for the direct
498 measurement of displacements in vibrating systems”, *Smart Materials and Structures*, Vol. 12 No.
499 5, pp. 785–794.

500 Wang, N., O’Malley, C., Ellingwood, B.R. and Zureick, A.-H. (2011), “Bridge Rating Using System
501 Reliability Assessment. I: Assessment and Verification by Load Testing”, *Journal of Bridge
502 Engineering*, Vol. 16 No. 6, pp. 854–862.

503 Xu, Y., Brownjohn, J.M.W., Hester, D. and Koo, K.Y. (2017), “Long-span bridges: Enhanced data
504 fusion of GPS displacement and deck accelerations”, *Engineering Structures*, Vol. 147, pp. 639–
505 651.

506 Yang, Y., Dorn, C., Mancini, T., Talken, Z., Kenyon, G., Farrar, C. and Mascareñas, D. (2017), “Blind
507 identification of full-field vibration modes from video measurements with phase-based video
508 motion magnification”, *Mechanical Systems and Signal Processing*, Elsevier, Vol. 85, pp. 567–
509 590.

510 Ye, X.W., Ni, Y.Q., Wai, T.T., Wong, K.Y., Zhang, X.M. and Xu, F. (2013), “A vision-based system

511 for dynamic displacement measurement of long-span bridges: algorithm and verification”, *Smart*
512 *Structures and Systems*, Vol. 12 No. 3_4, pp. 363–379.

513 Yoon, H., Elanwar, H., Choi, H., Golparvar-Fard, M. and Spencer, B.F. (2016), “Target-free approach
514 for vision-based structural system identification using consumer-grade cameras”, *Structural*
515 *Control and Health Monitoring*, Vol. 23 No. 12, pp. 1405–1416.

516 Zhao, X., Ri, K. and Wang, N. (2017), “Experimental Verification for Cable Force Estimation Using
517 Handheld Shooting of Smartphones”, *Journal of Sensors*, Vol. 2017, pp. 1–13.

518

519 TABLE CAPTIONS

520

521 Table 1 Tracking accuracy at 95% confidence interval for three tracking methods in laboratory conditions.

Tracking accuracy (95% confidence interval)	Correlation-based template matching	LK optical flow estimation	SIFT
Run 1 (pixel)	0.026±0.055	0.029±0.069	0.048±0.149
Run 2 (pixel)	-0.009±0.020	-0.001±0.020	0.011±0.037
Accuracy range (pixel)	[0.01, 0.08]	[0.02, 0.10]	[0.03, 0.20]

522

523

524

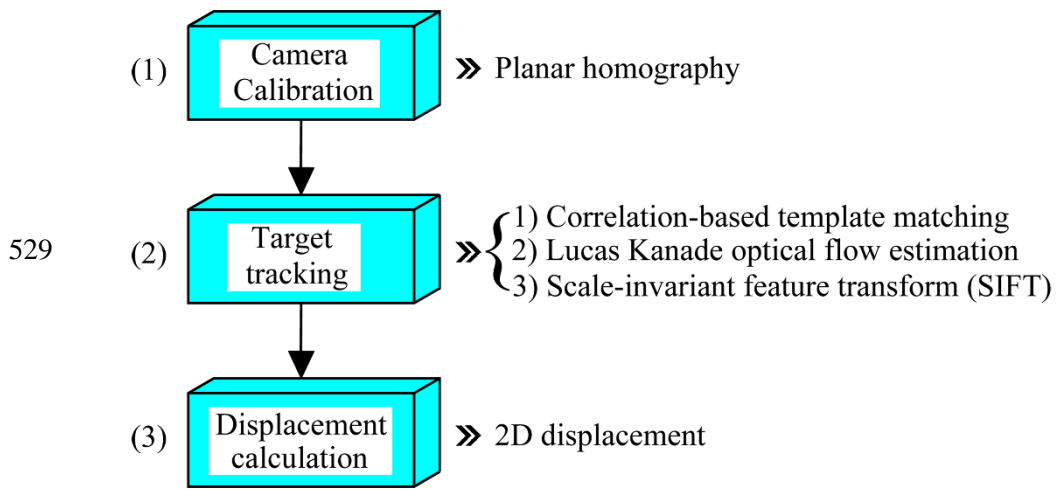
525 Table 2 Working performance of three tracking methods in field tests

Field conditions	Correlation-based template matching	LK optical flow estimation	SIFT
Long-range measurement	✓	✓	✓
Low-contrast patterns	✓	×	✓
Small pattern changes	×	✓	✓
Large pattern changes	×	×	×
Lighting changes	×	×	×

526

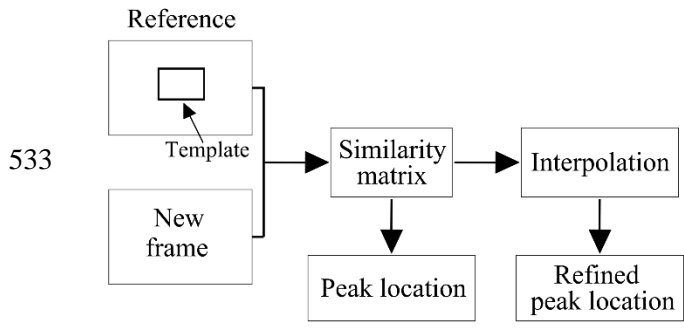
527

528 FIGURE CAPTIONS



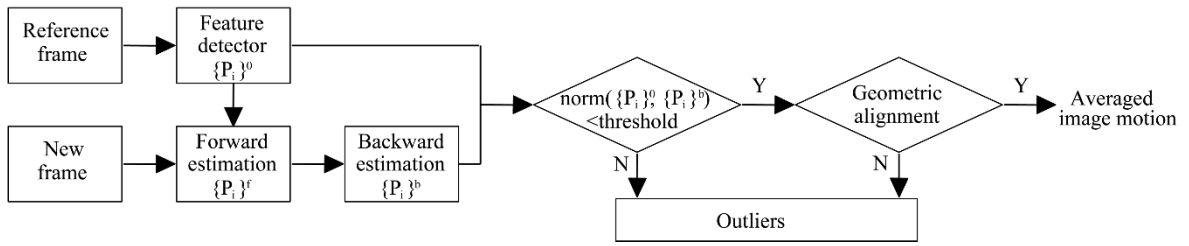
530

531 Figure 1 Procedures and methodologies in custom-developed video processing software package for structural
532 displacement measurement.



534 Figure 2 Procedures of one target tracking method: correlation-based template matching.

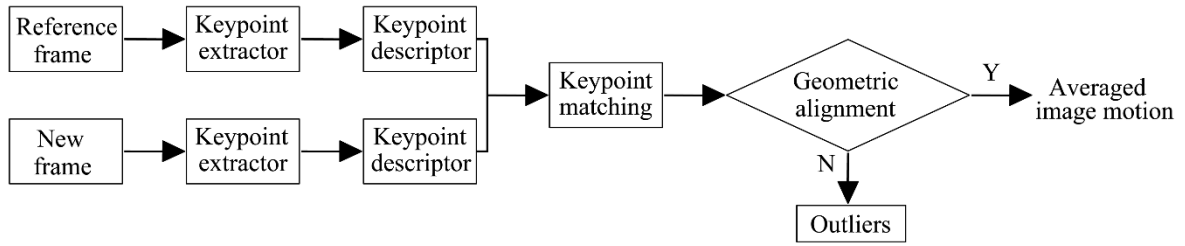
535



536

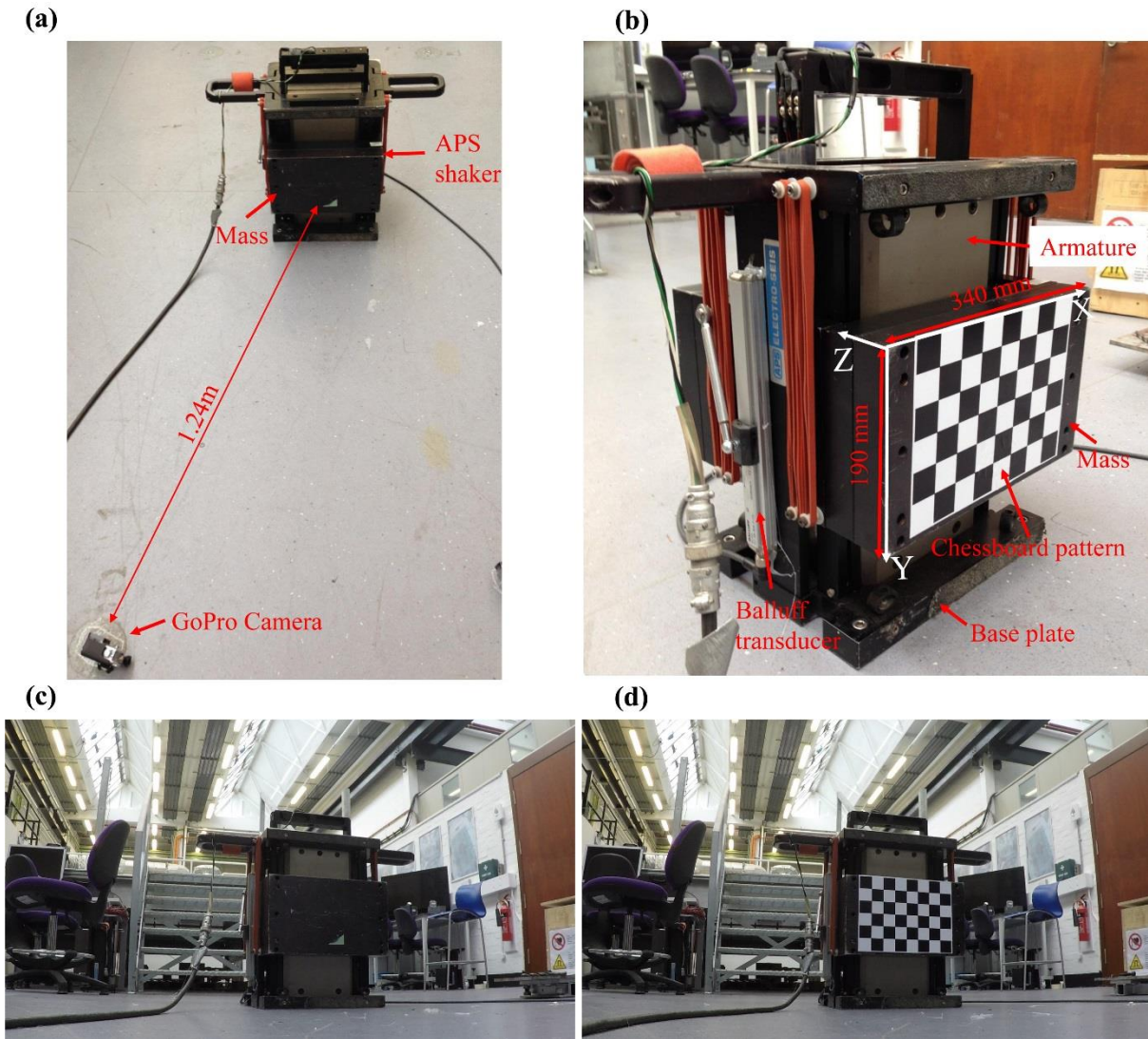
Figure 3 Procedures of one target tracking method: Lucas Kanade (LK) optical flow estimation.

537

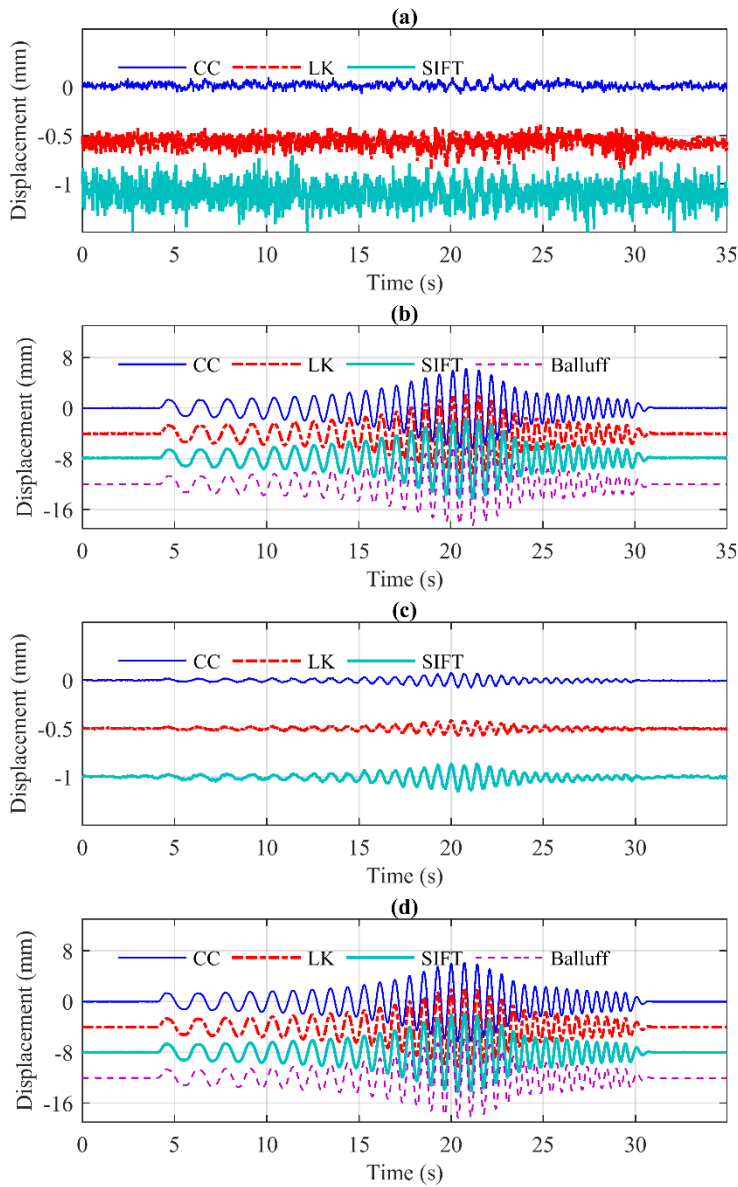


538 Figure 4 Procedures of one target tracking method: scale-invariant feature transform (SIFT).

539



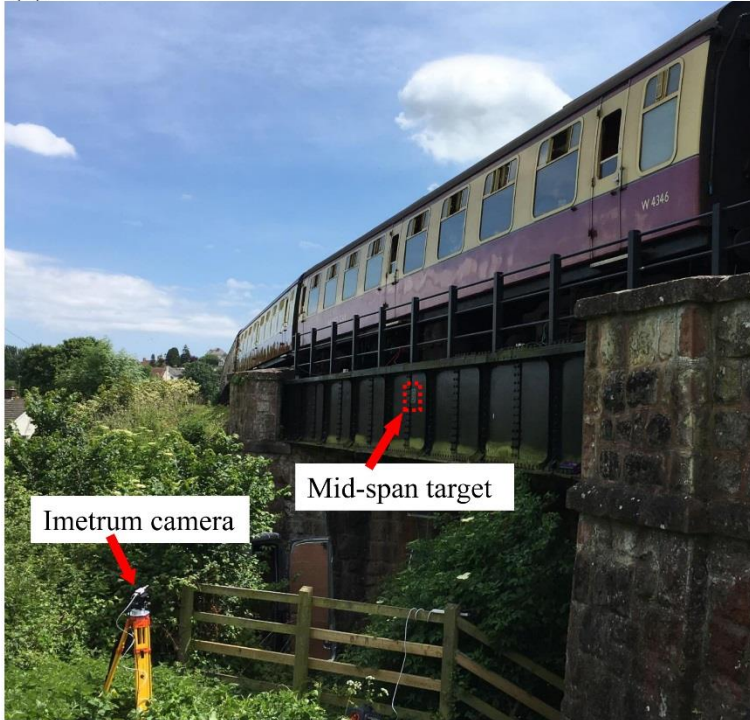
540 Figure 5 Test configuration of a vision-based system for vertical oscillation measurement of an APS shaker in
541 laboratory: (a) test configuration of shaker and GoPro camera in Run 1; (b) test configuration of shaker in Run 2
542 with chessboard patterns attached to shaker mass; (c) one sample frame from the GoPro video recorded in Run 1;
543 and (d) one sample frame from the GoPro video recorded in Run 2.



544

545 Figure 6 Time histories of displacement measurement of shaker mass acquired by the custom-developed video
 546 processing software package: (a) measured displacement in the horizontal direction by vision-based system in
 547 Run 1; (b) measured displacement in the vertical direction by vision-based system and Balluff transducer in Run
 548 1; (c) measured displacement in the horizontal direction by vision-based system in Run 2; and (d) measured
 549 displacement in the vertical direction by vision-based system and Balluff transducer in Run 2. (Legends CC, LK
 550 and SIFT denote the three target tracking methods used for video processing, namely correlation-based template
 551 matching, Lucas Kanda optical flow estimation and Scale-invariant feature transform.)

(a)

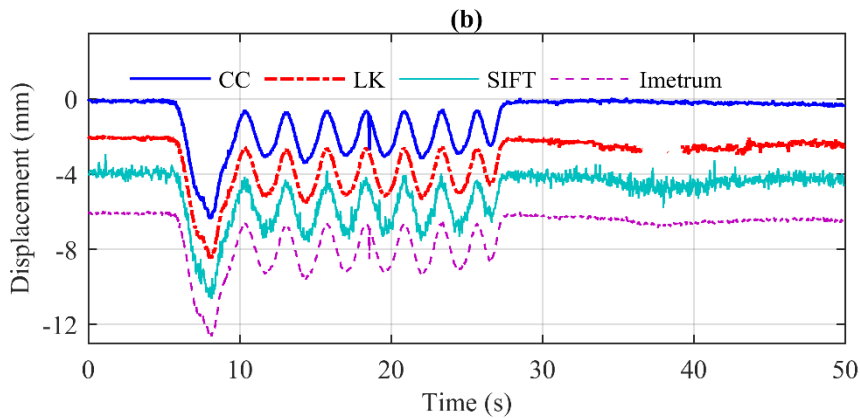
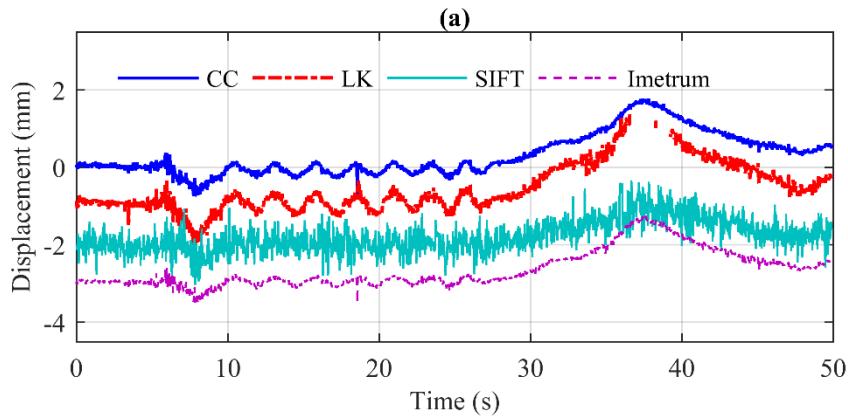


552

(b)



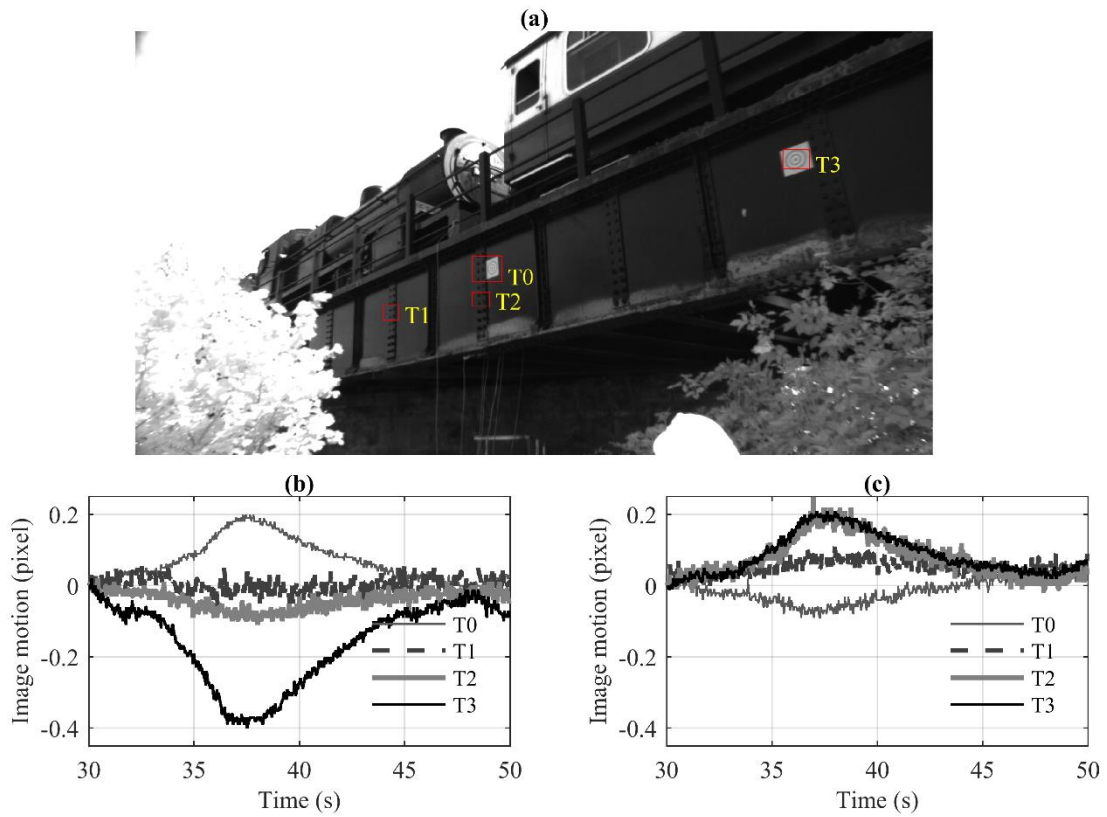
553 Figure 7 Test configuration of a vision-based system for the mid-span displacement measurement on a railway
554 bridge in Somerset, UK: (a) camera setup near the bridge and the target region at mid-span selected for video
555 tracking; and (b) one sample frame from the recorded video when one steam train passed through the bridge.



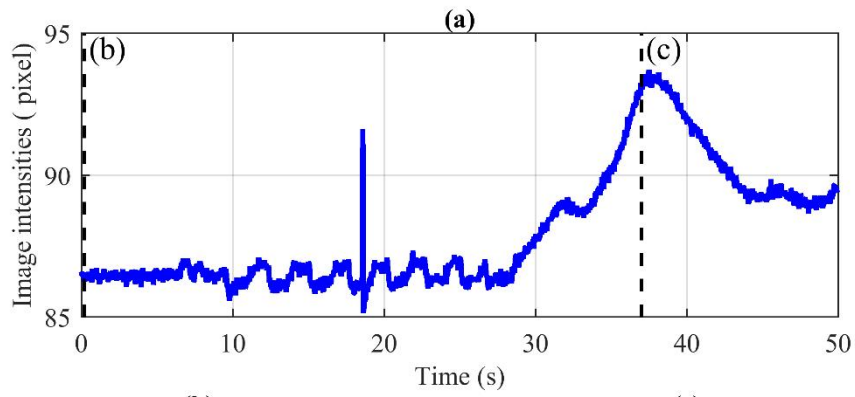
556

557 Figure 8 Time histories of displacement measurement acquired by the Imetrum system and by the custom-
 558 developed video processing software package using three tracking methods: (a) displacement measurement in the
 559 bridge longitudinal direction; and (b) displacement measurement in the vertical direction. (Legends CC, LK and
 560 SIFT denote the three target tracking methods used for video processing, namely correlation-based template
 561 matching, Lucas Kanda optical flow estimation and Scale-invariant feature transform.)

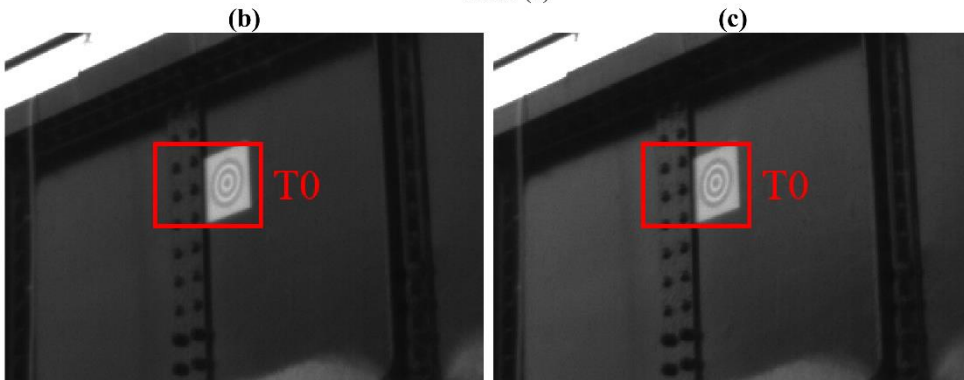
562



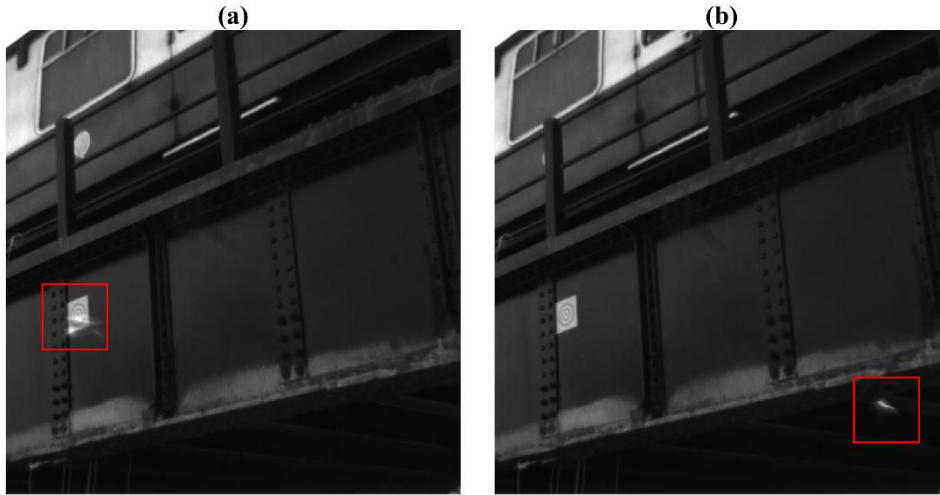
563 Figure 9 Tracking results of image motions at the selected four target regions (T0~T3) in the bridge girder by the
564 correlation-based template matching: (a) locations of four target regions in the frame selected for tracking; (b)
565 measured image motions at four target regions along the image horizontal direction; and (c) measured image
566 motions at four target regions along the image vertical direction.



567



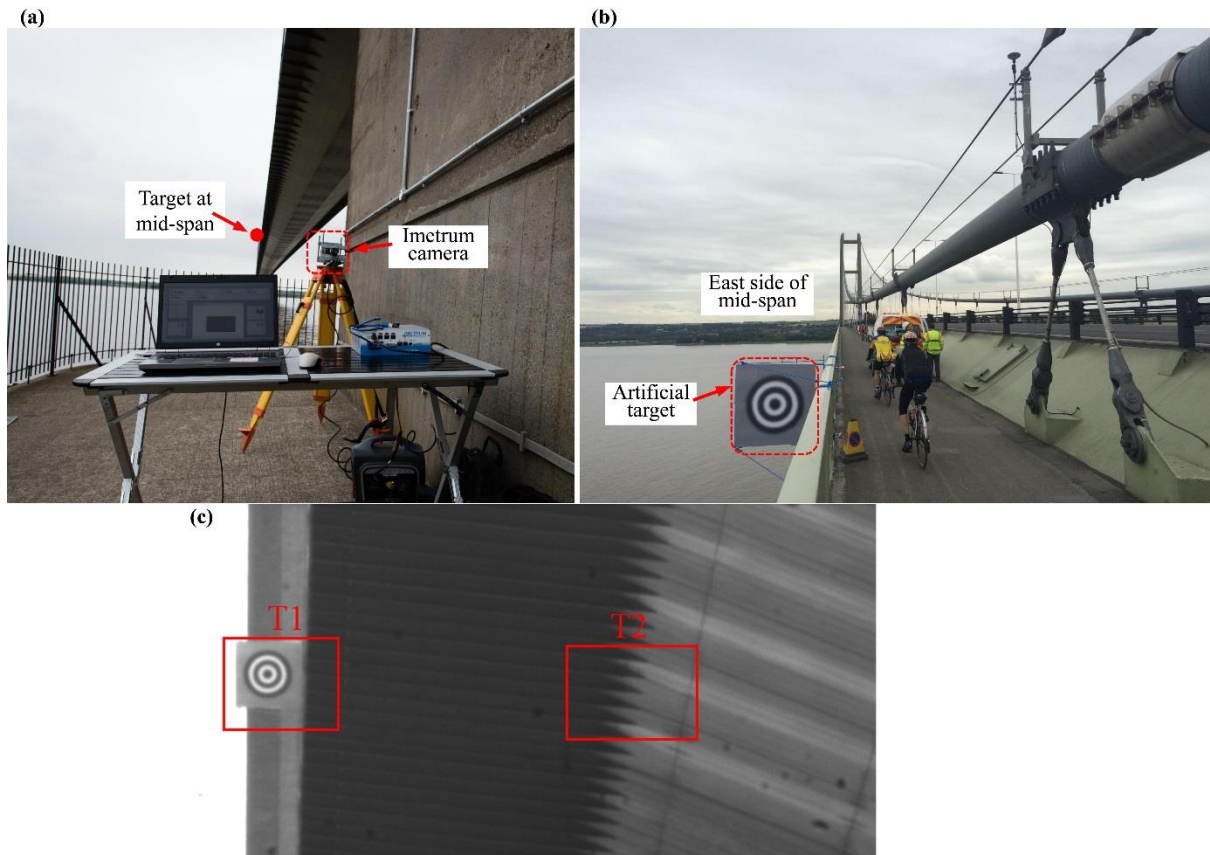
568 Figure 10 Variations of image brightness at the initially selected target region T0: (a) time history of mean pixel
 569 intensity at the target region T0; (b) the truncated initial frame with a rectangular annotation at the target region
 570 T0; and (c) the truncated frame at the time step of 37 s with a rectangular annotation at the target region T0.



571

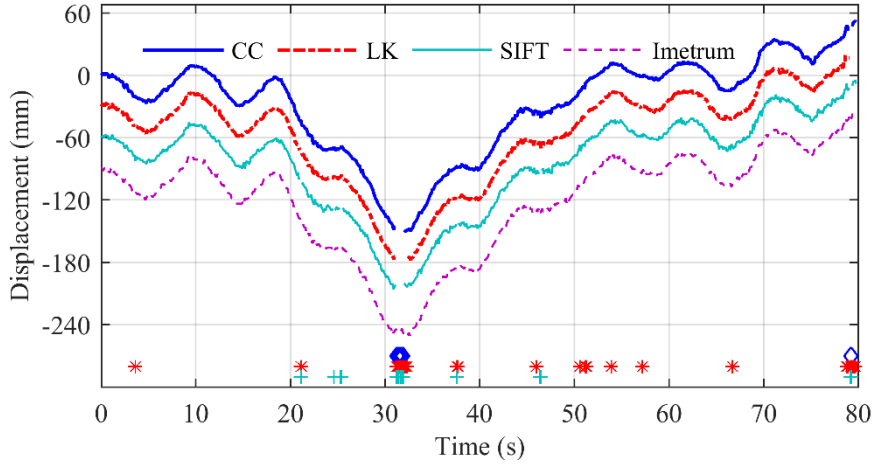
572 Figure 11 Two consecutive frames from video files at approx. 18.6 s indicating the changes of target pattern due
573 to a flying object (frames truncated and zoomed-in for clarification).

574

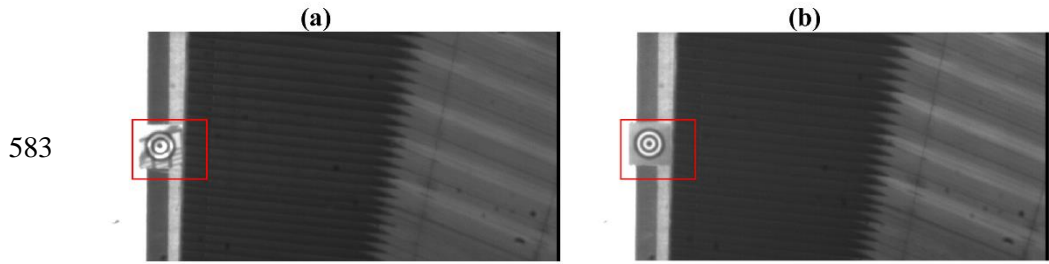


575 Figure 12 Test configuration of a vision-based system for the mid-span displacement measurement on the Humber
576 Bridge, UK (Xu et al., 2017): (a) camera setup near the bridge tower; (b) an artificial target installed at the east
577 side of mid-span; and (c) one sample frame from the recorded videos with the annotations at two selected target
578 regions for video tracking.

579

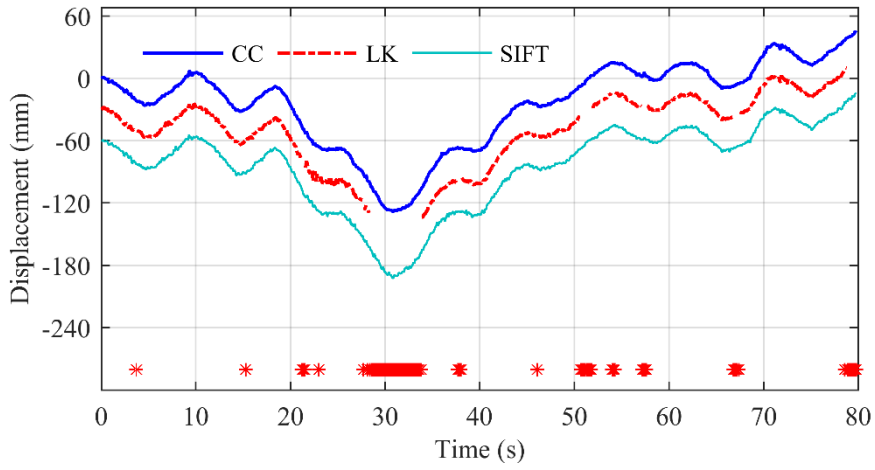


580 Figure 13 Time histories of displacement measurement in the vertical direction at the target region T1 acquired
581 by Imetrum system and by the custom-developed video processing software package using three tracking methods
582 with the markers indicating the time steps of tracking failure. (Legends have the same meaning as in Figure 8.)



584 Figure 14 Two frames from the video file at approx. 31.3 s indicating the changes of target pattern due to the
585 passing of one tall vehicle at the mid-span of the bridge that temporally blocked the sunlight, making the whole
586 target pattern visible in the image.

587



588 Figure 15 Time histories of displacement measurement in the vertical direction at the target region T2 acquired
589 by the custom-developed video processing software package using three tracking methods with the markers
590 indicating the time steps of tracking failure.